Analysis of Multiconductor Transmission Lines of Arbitrary Cross Section in Multilayered Uniaxial Media

Chung-I G. Hsu, *Member, IEEE,* Roger F. Harrington, *Life Fellow, IEEE,*
Krzysztof A. Michalski, *Senior Member, IEEE,* and Dalian Zheng, *Member, IEEE*

***Abstract*— A mixed-potential electric field integral equation is formulated and applied in conjunction with the method of moments to analyze a transmission-line system consisting of multiple conducting strips of arbitrary cross section embedded in a stratified medium with or without top and/or bottom ground planes. Each layer of the medium is possibly uniaxially anisotropic, with its optical axis perpendicular to the dielectric interfaces. Computed dispersion curves and modal currents are presented and, when possible, are compared with data available in the literature.**

I. Introduction

RECENT advances in integrated circuit technology have made microstrips, striplines, coplanar strips, and similar wave-guiding structures attractive not only in microwave and millimeter-wave applications, but also in high-speed digital computers. The conductors used as interconnects between VLSI devices may be very close to one another, which necessitates treating them as a single transmission line capable of supporting several modes, rather than several isolated transmission lines. The interconnects in modern microwave and millimeter-wave integrated circuits tend to have trapezoidal cross sections due to etching undercuts or as a result of the epitaxial growth process [1], [2], and cannot always be considered infinitely thin. These interconnects are supported by a dielectric substrate, which often exhibits uniaxial anisotropy, introduced in the manufacturing process [3].

Many numerical procedures have been successfully applied in the past two decades to obtain frequency-dependent characteristics of microstrips and striplines, but most of them are only applicable to (or optimized for) planar conducting strips of zero thickness (cf. [4], [5]–[17], to name just a few). Relatively few papers have considered laterally open microstrip structures with conductors of other cross section shapes, such as rectangular [18], trapezoidal [19], [20], circular [21], [22], or rectangular with semi-circular edges [23]. The concept of equivalent width has often been employed to approximately take into account the strip thickness [24]. However, it has recently been demonstrated, using a rigorous mixed-potential integral equation (MPIE) approach [19], that the dispersion curve for a finite-thickness microstrip lies below that of a microstrip with zero thickness, which is opposite to what is observed when the concept of equivalent width is used.

In this paper, we use an MPIE approach, which was originally developed for objects in isotropic media [25], [19], [26], and recently extended to objects in uniaxial media [27], to analyze a transmission-line system composed of multiple conductors of finite thickness and arbitrary cross section, embedded in a medium consisting of an arbitrary number of planar, possibly uniaxially anisotropic, dielectric layers. Computed dispersion curves and modal currents for bound modes are presented and, when possible, are compared with data available in the literature.

II. Formulation

The cross-sectional view of the structure under consideration is shown in Fig. 1. The medium consists of N planar, homogeneous dielectric layers, with the interfaces parallel to the xy plane. Each layer, say the nth, is characterized by permeability μ_{rn} and by transverse and longitudinal permittivities ϵ_{tn} and ϵ_{zn}, respectively, all relative to free space. The top layer of the medium may extend to $+\infty$ along the z axis, or be shielded by a ground plane made of a perfect electric conductor (PEC). Similarly, the bottom layer may extend to $-\infty$ along the z axis, or be shielded by a PEC ground plane. There are N_c PEC strips embedded in the layered medium, all uniform and of infinite extent along the y axis, but of arbitrary cross section shape. An $e^{j\omega t}$ time dependence is assumed and suppressed throughout.

Since we are interested in modes propagating in the y direction, we may assume that the phase factor $e^{-j\beta y}$ is common to all the fields and currents, where β is the propagation constant to be determined. Hence, we may express the surface current density as

$$\boldsymbol{J}(\boldsymbol{r}) = \boldsymbol{J}(\ell)e^{-j\beta y} \tag{1}$$

where ℓ is the arc-length coordinate on the contours of the conductor cross sections. By enforcing the condition that the

Manuscript received Dec. 30, 1992; revised Apr. 15, 1992. This work was supported in part by the U.S. Office of Naval Research (ONR) under Contract N00014-90-J-1197.

C. G. Hsu and R. F. Harrington are with the Department of Electrical and Computer Engineering, Syracuse University, Syracuse, NY 13244-1240.

K. A. Michalski is with the Electromagnetics & Microwave Laboratory, Department of Electrical Engineering, Texas A&M University, College Station, TX 77843-3128.

D. Zheng was with Texas A&M University. He is now with Integrated Engineering Software, Inc., 347-435 Ellice Ave., Winnipeg, Manitoba, Canada, R3B 1Y6.

IEEE Log Number 9204028.

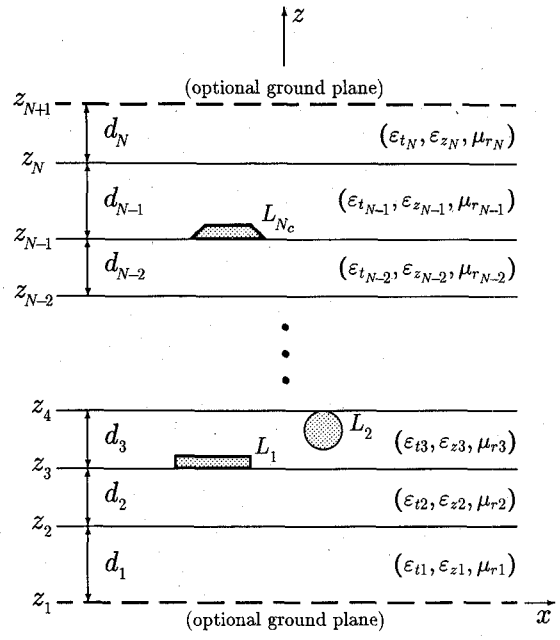

Fig. 1. Cross-sectional view of a multiconductor transmission line embedded in a stratified uniaxial medium.

tangential electric field must vanish at the surface of the conductors, we obtain an electric field integral equation (EFIE) of the form

$$\hat{\boldsymbol{u}}_n \times \sum_{i=1}^{N_c} \int_{L_i} \underline{\underline{\boldsymbol{G}}}^{EJ}(x,z|x',z') \cdot \boldsymbol{J}(\ell')\, d\ell' = 0, \quad \boldsymbol{r} \in L_n, n = 1,2,\cdots,N_c \tag{2}$$

where $\underline{\underline{\boldsymbol{G}}}^{EJ}(x,z|x',z')$, with $x \equiv x(\ell)$ and $z \equiv z(\ell)$, is the electric field dyadic Green's function of the layered medium [27], and where $\hat{\boldsymbol{u}}_n$ denotes an outward unit vector normal to the boundary L_n of the nth conductor. In the above and throughout, primed quantities denote source coordinates, unit vectors are distinguished by carets, and dyadics by double underlines.

The severe source-region singularity of the kernel of the EFIE (2) makes it unsuitable for a direct application of the method of moments [28], [29]. Hence, we first transform it into the MPIE form,

$$\hat{\boldsymbol{u}}_n \times \sum_{i=1}^{N_c} \{\boldsymbol{A}_i(x,z) + (\boldsymbol{\nabla}_\ell - \hat{\boldsymbol{y}} j\beta)\Phi_i(x,z)\} = 0, \quad \boldsymbol{r} \in L_n, n = 1,2,\cdots,N_c \tag{3}$$

where $\boldsymbol{\nabla}_\ell$ is the transverse (to y) part of the operator nabla, and where

$$\boldsymbol{A}_i(x,z) = \int_{L_i} \underline{\underline{\boldsymbol{K}}}^{A}(x,z|x',z') \cdot \boldsymbol{J}(\ell')\, d\ell' \tag{4}$$

and

$$\Phi_i(x,z) = \int_{L_i} K^{\phi}(x,z|x',z')(\boldsymbol{\nabla}'_\ell - \hat{\boldsymbol{y}} j\beta) \cdot \boldsymbol{J}(\ell')\, d\ell' \tag{5}$$

are the magnetic vector potential and the electric scalar potential, respectively, due to the surface current on the ith conductor. These potentials are not unique, as discussed in [30], [26], [27]. In the latter reference, two different MPIE formulations, referred to as the "traditional" and the "alternative," are developed for arbitrarily shaped conductors in layered uniaxial media.

The expressions for the dyadic kernel $\underline{\underline{\boldsymbol{K}}}^{A}$ and the scalar kernel K^{ϕ} comprise improper spectral integrals of the form

$$S_{sn}^{cn}\{f(k_x)\} = \frac{1}{\pi}\int_0^\infty f(k_x) \cdot \begin{bmatrix} \cos k_x(x-x') \\ \sin k_x(x-x') \end{bmatrix} k_x^n\, dk_x \tag{6}$$

where k_x is the Fourier transform domain counterpart of x, and where the subscripts c and s are associated with the cosine and sine functions, respectively, and n assumes the values 0 or 1. Using this notation, the nonzero elements of $\underline{\underline{\boldsymbol{K}}}^{A}$ and K^{ϕ} for the traditional MPIE formulation [31], [27] can be expressed as

$$K^A_{xx}(x,z|x',z') = S_{c0}\{V^h_{i,mn}(z|z')\} \tag{7}$$

$$K^A_{zx}(x,z|x',z') = -jk_0\eta_0 \mathcal{S}_{s1}\left\{\frac{\mu_{rm}}{k_\rho^2}[I^h_{i,mn}(z|z') - I^e_{i,mn}(z|z')]\right\} \tag{8}$$

$$K^A_{zy}(x,z|x',z') = \beta k_0\eta_0 \mathcal{S}_{c0}\left\{\frac{\mu_{rm}}{k_\rho^2}[I^h_{i,mn}(z|z') - I^e_{i,mn}(z|z')]\right\} \tag{9}$$

$$K^A_{xz}(x,z|x',z') = -jk_0\eta_0 \mathcal{S}_{s1}\left\{\frac{\mu_{rn}}{k_\rho^2}[V^h_{v,mn}(z|z') - V^e_{v,mn}(z|z')]\right\} \tag{10}$$

$$K^A_{yz}(x,z|x',z') = \beta k_0\eta_0 \mathcal{S}_{c0}\left\{\frac{\mu_{rn}}{k_\rho^2}[V^h_{v,mn}(z|z') - V^e_{v,mn}(z|z')]\right\} \tag{11}$$

$$K^A_{zz}(x,z|x',z') = \eta_0^2 \mathcal{S}_{c0}\left\{\left[\frac{\mu_{rm}}{\epsilon_{zn}} - \frac{\mu_{rn}}{\epsilon_{tm}}\left(\frac{k^e_{zm}}{k_\rho}\right)^2\right] I^e_{v,mn}(z|z') + \mu_{rm}\mu_{rn}\left(\frac{k_0}{k_\rho}\right)^2 I^h_{v,mn}(z|z')\right\} \tag{12}$$

$$K^{\phi}(x,z|x',z') = \mathcal{S}_{c0}\left\{\frac{1}{k_\rho^2}[V^h_{i,mn}(z|z') - V^e_{i,mn}(z|z')]\right\} \tag{13}$$

where η_0 and k_0 denote, respectively, the intrinsic impedance and wavenumber of free space, and $k_\rho^2 = k_x^2 + \beta^2$. The subscripts m and n in the above indicate that the observation point (x,z) is in the mth layer, and the source point (x',z') in the nth layer. In deriving (7)–(13), use has been made of the transmission-line network analogue of the layered medium [32, ch. 2], which is illustrated in Fig. 2 for a three-layer geometry. This network actually represents two networks (having identical configurations, but in general different propagation constants and characteristic impedances) that arise from the decomposition of the electromagnetic field into partial fields that are transverse-magnetic (TM) and transverse-electric (TE) to $\hat{z}$ [32], [33]. The superscript p in Fig. 2 stands for e or h,

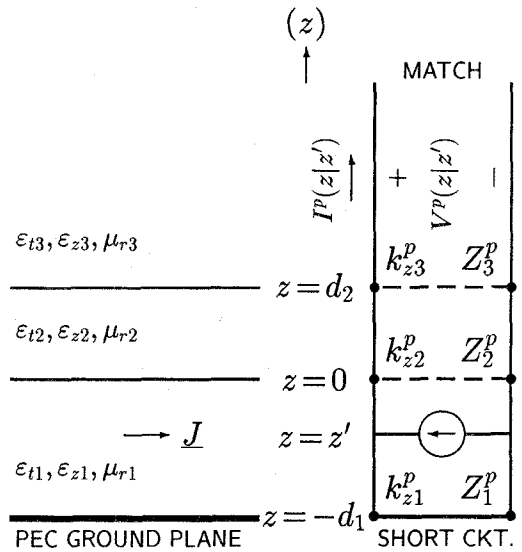

Fig. 2. Transmission-line analogue of a layered medium.

which designate, respectively, the quantities associated with the TM and TE networks. The propagation constants of the nth transmission line section are found as

$$k_{zn}^e = \sqrt{k_0^2 \epsilon_{tn} \mu_{rn} - \frac{\epsilon_{tn}}{\epsilon_{zn}} k_\rho^2},$$
$$k_{zn}^h = \sqrt{k_0^2 \epsilon_{tn} \mu_{rn} - k_\rho^2} \tag{14}$$

where the branch of the square root is determined by the condition that $\mathrm{Im}\{k_{zn}^p\} < 0$. The corresponding characteristic impedances (and admittances) are given as

$$Z_n^e \equiv \frac{1}{Y_n^e} = \frac{\eta_0 k_{zn}^e}{k_0 \epsilon_{tn}}, \quad Z_n^h \equiv \frac{1}{Y_n^h} = \frac{k_0 \eta_0 \mu_{rn}}{k_{zn}^h}. \tag{15}$$

In (7)–(13), $V_{i,mn}^p(z|z')$ and $I_{i,mn}^p(z|z')$ denote, respectively, the voltage and current at z on the mth transmission line section, due to a 1 A current source at z' on the nth line section. Similarly, $V_{v,mn}^p(z|z')$ and $I_{v,mn}^p(z|z')$ denote, respectively, the voltage and current at z on the mth transmission line section, due to a 1 V voltage source at z' on the nth section. These transmission-line Green's functions are derived in the Appendix for a medium with an arbitrary number of layers.

III. Numerical Method

In this section, the method of moments [28], [29] is employed to solve the MPIE (3) for the multiconductor transmission-line problem of Fig. 1. As the first step of the numerical procedure, we approximate the cross section contours of the conductors by piecewise linear segments, as illustrated in Fig. 3. The arc-length coordinate ℓ will now be associated with the approximated contours, instead of the original ones. The method of moments requires that the unknown currents be expanded in terms of a set of known basis functions with unknown coefficients, viz:

$$\boldsymbol{J}_t^p(\ell) = \sum_j I_j^{p,t} \boldsymbol{\Lambda}_j^p(\ell),$$
$$J_y^p(\ell) = \sum_j I_j^{p,y} \Pi_j^p(\ell), \qquad p = 1, 2, \cdots, N_c \tag{16}$$

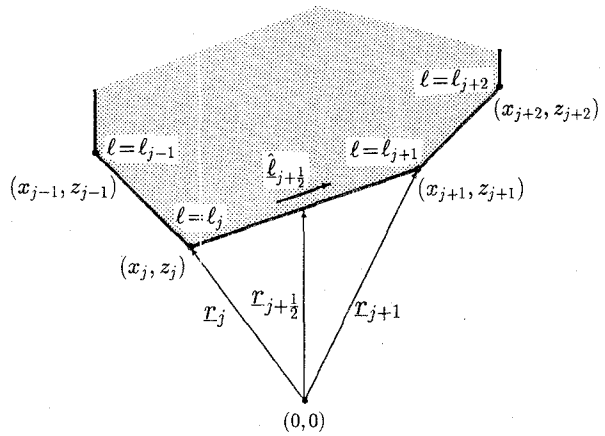

Fig. 3. Linear segmentation model of a contour.

where

$$\boldsymbol{\Lambda}_j^p(\ell) = \begin{cases} \hat{\boldsymbol{\ell}}_{j-(1/2)}^p \dfrac{\ell - \ell_{j-1}^p}{\ell_j^p - \ell_{j-1}^p}, & \ell_{j-1}^p < \ell < \ell_j^p \\ \hat{\boldsymbol{\ell}}_{j+(1/2)}^p \dfrac{\ell_{j+1}^p - \ell}{\ell_{j+1}^p - \ell_j^p}, & \ell_j^p < \ell < \ell_{j+1}^p \\ 0, & \text{otherwise} \end{cases} \tag{17}$$

with

$$\hat{\boldsymbol{\ell}}_{j+(1/2)}^p = \frac{\boldsymbol{r}_{j+1}^p - \boldsymbol{r}_j^p}{\Delta_{j+1}^p}, \quad \Delta_{j+1}^p = |\boldsymbol{r}_{j+1}^p - \boldsymbol{r}_j^p| \tag{18}$$

and

$$\Pi_j^p(\ell) = \begin{cases} 1, & \ell_{j-1}^p < \ell < l_j^p \\ 0, & \text{otherwise.} \end{cases} \tag{19}$$

In the above expressions, the subscript j and the superscript p signify quantities related to the jth expansion function or segment on the pth conductor (the superscript p is omitted in Fig. 3 for simplicity).

The MPIE (3) is next tested with $\hat{\boldsymbol{y}}\Pi_i^p$ and $\boldsymbol{\Lambda}_i^p$. In this process, the transverse nabla operator in (3) is transferred to operate on the testing function by applying Green's first identity, viz:

$$\int \boldsymbol{\Lambda}_i^p(\ell) \cdot \nabla_\ell \Phi(x,z)\, d\ell$$
$$= -\int [\nabla_\ell \cdot \boldsymbol{\Lambda}_i^p(\ell)] \Phi(x,z)\, d\ell$$
$$= -\int \left[\frac{\Pi_i^p(\ell)}{\Delta_i^p} - \frac{\Pi_{i+1}^p(\ell)}{\Delta_{i+1}^p} \right] \Phi(x,z)\, d\ell. \tag{20}$$

To save computer time, the following approximations are used in the testing procedure:

$$\int \Pi_i^p(\ell)\, f(\ell)\, d\ell \approx \Delta_i^p f(\ell_{i-(1/2)}^p) \tag{21}$$

$$\int \boldsymbol{\Lambda}_i^p(\ell)\, f(\ell)\, d\ell \approx \tfrac{1}{2} [\hat{\boldsymbol{\ell}}_{i-(1/2)}^p \Delta_i^p f(\ell_{i-(1/2)}^p) + \hat{\boldsymbol{\ell}}_{i+(1/2)}^p \Delta_{i+1}^p f(\ell_{i+(1/2)}^p))] \tag{22}$$

where $f(\ell)$ represents the scalar potential $\Phi(x,z)$, or a component of the vector potential $\boldsymbol{A}(x,z)$, and where $\ell_{i+(1/2)}^p$ is

the arc-length coordinate of a point specified by the position vector (cf. Fig. 3)

$$\boldsymbol{r}^p_{i+(1/2)} = \hat{\boldsymbol{x}} x^p_{i+(1/2)} + \hat{\boldsymbol{z}} z^p_{i+(1/2)} = \frac{\boldsymbol{r}^p_i + \boldsymbol{r}^p_{i+1}}{2}. \tag{23}$$

Furthermore, when computing the magnetic vector potential due to $\boldsymbol{\Lambda}^p_j$, we approximate the resulting integral as

$$\begin{aligned}\int \underline{\underline{\boldsymbol{K}}}^A(x,z|x',z') \cdot \boldsymbol{\Lambda}^p_j(\ell')\, d\ell' \\ \approx \tfrac{1}{2} \int \underline{\underline{\boldsymbol{K}}}^A(x,z|x',z') \\ \cdot [\hat{\boldsymbol{\ell}}^p_{j-(1/2)} \Pi^p_j(\ell') + \hat{\boldsymbol{\ell}}^p_{j+(1/2)} \Pi^p_{j+1}(\ell')]\, d\ell'.\end{aligned} \tag{24}$$

As a final step, we substitute the expansions (16) into the tested form of (3) to convert it into a homogeneous matrix equation for the current expansion coefficients. Assuming, for simplicity, that there are only two conductors, this equation has the form

$$\begin{bmatrix} [Z^{11,tt}_{ij}] & [Z^{11,ty}_{ij}] & [Z^{12,tt}_{ij}] & [Z^{12,ty}_{ij}] \\ [Z^{11,yt}_{ij}] & [Z^{11,yy}_{ij}] & [Z^{12,yt}_{ij}] & [Z^{12,yy}_{ij}] \\ [Z^{21,tt}_{ij}] & [Z^{21,ty}_{ij}] & [Z^{22,tt}_{ij}] & [Z^{22,ty}_{ij}] \\ [Z^{21,yt}_{ij}] & [Z^{21,yy}_{ij}] & [Z^{22,yt}_{ij}] & [Z^{22,yy}_{ij}] \end{bmatrix} \cdot \begin{bmatrix} [I^{1,t}_j] \\ [I^{1,y}_j] \\ [I^{2,t}_j] \\ [I^{2,y}_j] \end{bmatrix} = \begin{bmatrix} [0] \\ [0] \\ [0] \\ [0] \end{bmatrix} \tag{25}$$

with the matrix elements given as

$$\begin{aligned} Z^{pq,tt}_{ij} =& \frac{\Delta^p_i}{4}(A^{pq,tt}_{i,j} + A^{pq,tt}_{i,j+1}) + \frac{\Delta^p_{i+1}}{4} \\ & \cdot (A^{pq,tt}_{i+1,j} + A^{pq,tt}_{i+1,j+1}) - \frac{1}{\Delta^q_j}(\Phi^{pq}_{i,j} - \Phi^{pq}_{i+1,j}) \\ & + \frac{1}{\Delta^q_{j+1}}(\Phi^{pq}_{i,j+1} - \Phi^{pq}_{i+1,j+1}) \end{aligned} \tag{26}$$

$$\begin{aligned} Z^{pq,ty}_{ij} =& \frac{\Delta^p_i}{2} A^{pq,ty}_{i,j} + \frac{\Delta^p_{i+1}}{2} A^{pq,ty}_{i+1,j} \\ & + j\beta(\Phi^{pq}_{i,j} - \Phi^{pq}_{i+1,j}) \end{aligned} \tag{27}$$

$$\begin{aligned} Z^{pq,yt}_{ij} =& \frac{\Delta^p_i}{2}(A^{pq,yt}_{i,j} + A^{pq,yt}_{i,j+1}) \\ & - j\beta\left(\frac{\Delta^p_i}{\Delta^q_j}\Phi^{pq}_{i,j} - \frac{\Delta^p_i}{\Delta^q_{j+1}}\Phi^{pq}_{i,j+1}\right) \end{aligned} \tag{28}$$

$$Z^{pq,yy}_{ij} = \Delta^p_i A^{pq,yy}_{i,j} - \beta^2 \Delta^p_i \Phi^{pq}_{i,j} \tag{29}$$

where the index j, when used as a subscript, should not be confused with the imaginary unit. In (26)–(29), we have introduced the notation

$$\begin{aligned} A^{pq,\tau\eta}_{ij} = & \int_{\ell^q_{j-1}}^{\ell^q_j} \hat{\tau} \cdot \underline{\underline{\boldsymbol{K}}}^A(x^p_{i-(1/2)}, z^p_{i-(1/2)}|x',z') \\ & \cdot \hat{\boldsymbol{\eta}}\, d\ell' \end{aligned} \tag{30}$$

$$\Phi^{pq}_{ij} = \int_{\ell^q_{j-1}}^{\ell^q_j} K^\phi(x^p_{i-(1/2)}, z^p_{i-(1/2)}|x',z')\, d\ell' \tag{31}$$

where $(\tau,\eta) = (t,y)$, and $\hat{\boldsymbol{t}} \equiv \hat{\boldsymbol{t}}(\ell) = \hat{\boldsymbol{\ell}}^p_{j+(1/2)}$ for $\ell^p_j < \ell < \ell^p_{j+1}$. In the general case with N_c conductors, the matrix in (25) comprises $4N_c^2$ blocks of submatrices.

The kernel functions in the above have been defined by the spectral integrals (7)–(13), which are evaluated by a composite Gauss quadrature. To accelerate the convergence of these integrals, we first subtract from the integrands their large argument asymptotic forms. Furthermore, when $|x - x'|$ is larger than $|z - z'|$, we also employ the method of averages [25], [34]. Finally, the closed-form integrals of the asymptotic forms are added back to compensate for the subtracted terms. The former explicitly exhibit their source-region logarithmic singularities, which are integrable and are easily taken care of in evaluating the kernel integrals (30)–(31).

The equation (25) has nontrivial solutions only for those values of β, which make the matrix determinant vanish. These values are found by the Müller method [35], and the corresponding modal current coefficients are then determined from (25).

IV. Numerical Results

In this section, we present sample numerical results for the propagation constants and modal current distributions for a variety of transmission-line configurations. In all examples considered, the media are assumed lossless and nonmagnetic (i.e., $\mu_{rn} = 1$ for all layers). Some of the structures analyzed comprise both uniaxial and isotropic dielectric layers. If a layer is isotropic, its relative permittivity is denoted by ϵ_r. Only the proper, bound modes, which propagate unattenuated with a real propagation constant β, are considered. The dispersion curves are given either for β/k_0, or for the effective dielectric constant $\epsilon_{\text{eff}} = (\beta/k_0)^2$.

In Fig. 4, we present dispersion curves for a circular-wire transmission line embedded in a grounded two-layer isotropic medium with or without a top ground plane. The latter configuration was first analyzed by Faché and De Zutter [21], using an approach especially developed for wire conductors, and their results are shown by square symbols in Fig. 4. In this figure, ϵ_{eff} is plotted versus the electrical thickness of the substrate, d/λ_0, where λ_0 is the free-space wavelength. The wire is completely embedded in the dielectric slab for $h/d = 0.75$ or 0.5, and in the air region when $h/d = 1.25$ or 1.5. In the analysis, the circular cross section contour of the wire was approximated by sixteen linear segments of equal length. We note that the results for $B/d = \infty$ (unshielded structure) are indistinguishable from those for $B/d = 10$. This is to be expected, since the field of the bound mode is mainly trapped in the substrate and near the conductor. The presence of the top ground plane presents a noticeable disturbance to the bound wave only if it is close to the conductor or to the dielectric interface.

In Fig. 5, we present dispersion curves for a three-conductor microstrip transmission line, which supports three fundamental modes. The dielectric is made of ceramic-impregnated teflon, known as Epsilam 10, which is uniaxial, with $\epsilon_t = 13$ and $\epsilon_z = 10.2$. As a check for the computer code, we have further divided the dielectric slab into two layers. Two configurations

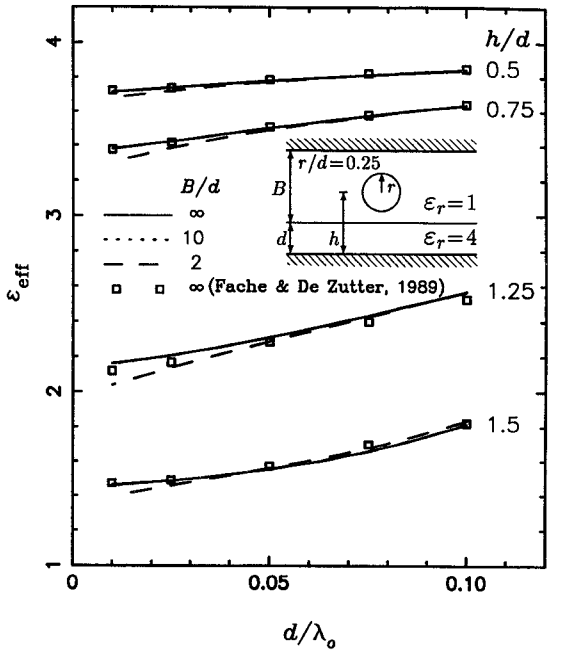

Fig. 4. Dispersion curves for a circular-wire transmission line.

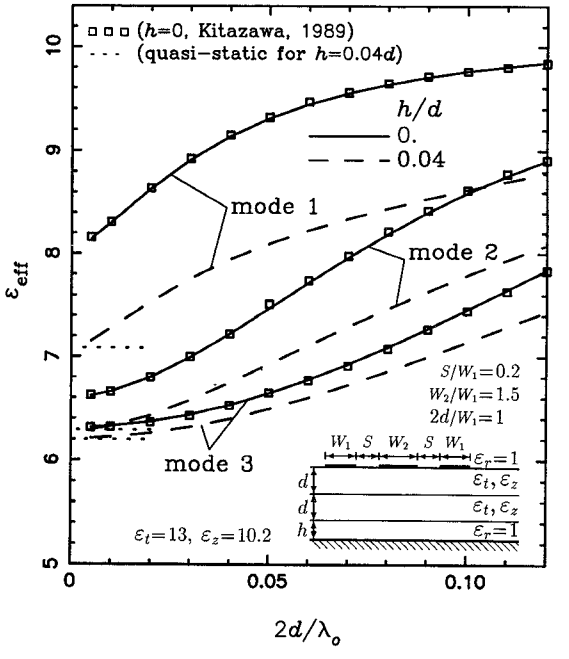

Fig. 5. Dispersion curves for a three-strip microstrip transmission line.

have been analyzed, one without an air gap ($h/d = 0$), and the other with an air gap ($h/d = 0.04$), and the corresponding results are shown in solid and dashed lines, respectively. These configurations have been previously analyzed by Kitazawa [15], the first done by a full-wave method (square symbols), and the second by a quasistatic approach (dotted lines). It is of interest to note that a small air gap between the ground plane and the dielectric slab results in big changes in the dispersion curves. The longitudinal (transverse) current distributions for modes 1, 2, and 3 are found to be even (odd), odd (even), and even (odd), respectively.

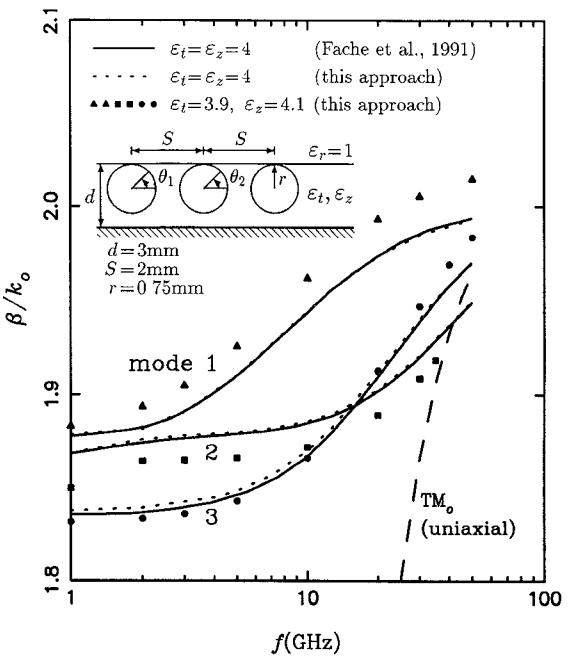

Fig. 6. Dispersion curves for a three-wire transmission line.

In Fig. 6, we present dispersion curves for a three-wire transmission line embedded in a grounded dielectric slab, which supports three fundamental modes. The solid lines represent the results computed by Faché *et al.* [22] for the case of an isotropic substrate ($\epsilon_r = 4$), whereas our results for the same substrate are illustrated by the dotted lines. Note that a logarithmic scale is used for the frequency. Our results for a uniaxial substrate, where $\epsilon_t = 3.9$ and $\epsilon_z = 4.1$, are indicated by three different symbols. As can be seen from the figure, even this slight anisotropy has a noticeable effect on the dispersion curves. In the isotropic case, all three modes remain in the bound regime in the frequency range considered. In the uniaxial case, mode 2 enters the leaky regime [36] at a frequency between 30 to 40 GHz, above which the dominant slab mode, indicated as TM_0 in Fig. 6, is excited. The dispersion curve of the latter is obtained by finding the zero of (34) (see the appendix). The longitudinal and transverse modal current distributions at $f = 10$ GHz are shown in Fig. 7. For modes 1, 2, and 3, the longitudinal (transverse) currents are even (odd), even (odd), and odd (even), respectively. Because of this symmetry property, we only plot the currents on the left and center conductors. We note that the longitudinal and transverse currents are in phase quadrature, which is characteristic of bound modes on lossless transmission lines.

We next consider three transmission line structures, which differ in the cross section shape of the conductors, as illustrated in Fig. 8. The cross sections of the conductors are (a) trapezoidal (which may arise as a result of an epitaxial growth process), (b) rectangular (the ideal case), and (c) inverted trapezoidal (which may be due to etching undercuts). The dispersion curves for the three fundamental modes that each of the three transmission lines may support are plotted in Fig. 9. The longitudinal (transverse) current distributions for modes 1, 2, and 3 are found to be even (odd), odd (even), and even

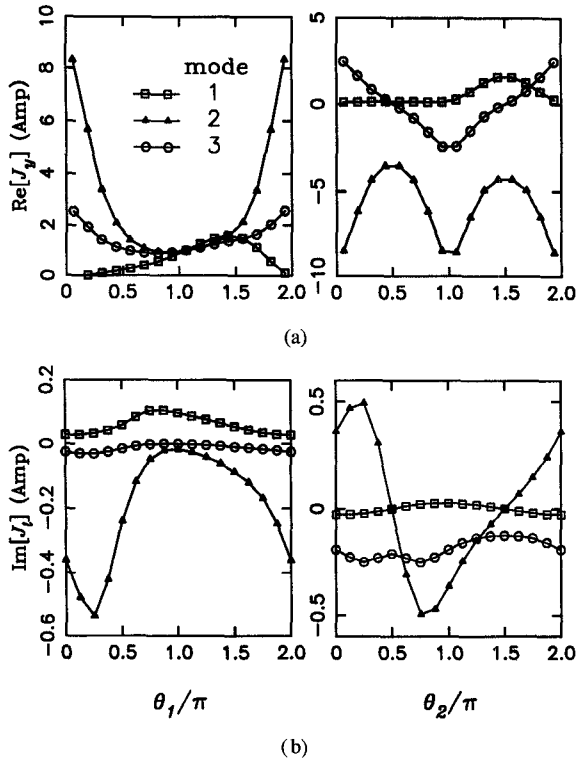

Fig. 7. (a) Longitudinal and (b) transverse current distributions at $f = 10$ GHz for the three-wire transmission line in the configuration of Fig. 6, with $\epsilon_t = 3.9$ and $\epsilon_z = 4.1$.

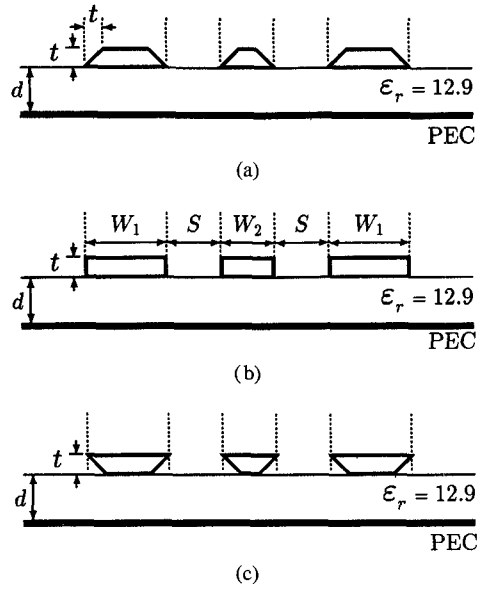

Fig. 8. Geometry of three transmission line configurations with conductors of (a) trapezoidal, (b) rectangular, and (c) inverted trapezoidal cross section. The dimensions are $d = 120\mu$m, $W_1 = 15\mu$m, $W_2 = S = 10\mu$m, and $t = 3\mu$m.

(odd), respectively. In Fig. 9, we also show the quasistatic results obtained by Schroeder and Wolff [2] for the same transmission lines, but having a finite-width substrate. We observe that the dispersion curves for configurations (a) and (b) differ less than those for (b) and (c). This is expected, since in the former two geometries the conductor widths adjacent to the dielectric slab (where there is a highly concentrated field)

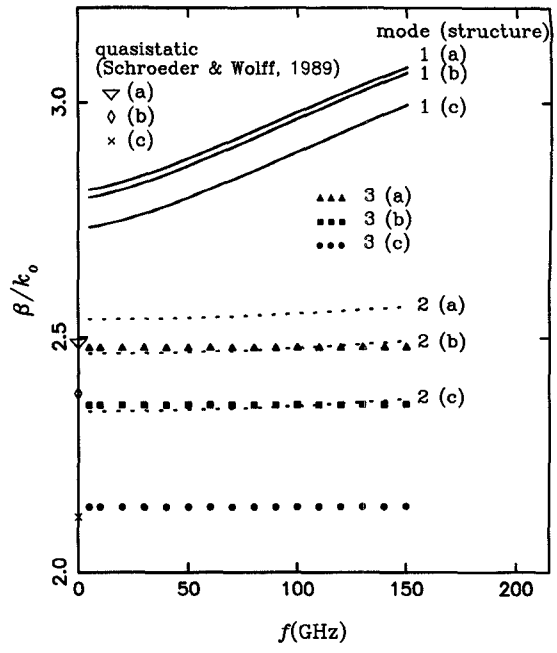

Fig. 9. Dispersion curves of modes 1, 2, and 3 for the transmission line configurations (a), (b), and (c) of Fig. 8. The quasistate results of Schroeder and Wolff are for a structure with a substrate of a finite width of 130 μm.

are the same. We also note that the quasistatic results of [2] are very close to the low-frequency limits of mode 3 of our results. However, it is not clear from [2] to which mode these quasistatic values correspond.

In Fig. 10, we present dispersion curves for a two-strip transmission line in an unshielded medium comprising both uniaxial and isotropic layers (see the inset). Since there are only two conductors and there are no ground planes in this structure, we expect it to have only one noncutoff fundamental mode (called mode 1 in Fig. 10). Nevertheless, an additional noncutoff mode (called mode 2) has been found. In addition to the dispersion curves of these two modes, we also plot in Fig. 10 the dispersion curves of the first two slab modes (indicated as TE_0 and TM_0), computed from (34) of the Appendix. The longitudinal currents of mode 1 on the two strips (not shown) are found to be in different directions, whereas those of mode 2 are in the same direction. Hence, mode 2 is similar to the fundamental mode of a coated conducting cylinder, where the surface current on the circumference of the cylinder flows in the same direction, and whose suitability as a single-conductor transmission line was studied by Goubau [37]. A salient feature of this Goubau mode is that its ϵ_{eff} is very close at low frequencies to that of free space, and that its field is very loosely bound to the dielectric. In fact, when we replace the two strips in the configuration shown in Fig. 10 by a single strip, we still can find a mode, which behaves similarly to the aforementioned mode 2.

V. Conclusion

A mixed-potential integral equation (MPIE) formulation has been implemented in conjunction with the method of moments to compute the propagation constants and modal currents of a multiconductor transmission line embedded in a laterally open

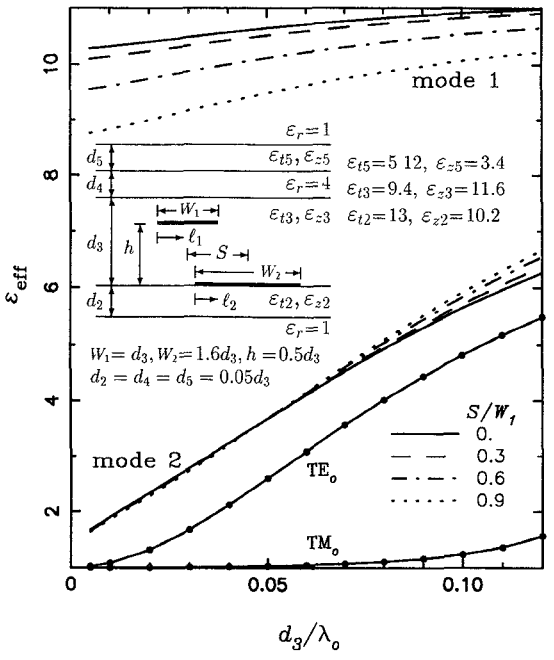

Fig. 10. Dispersion curves for a two-strip transmission line in an unshielded layered medium.

multilayered uniaxial medium. The approach is general and flexible, and can handle both open and shielded structures. It is applicable to conductors of arbitrary cross section, including trapezoidal, which often arises in practice due to underetching or as a result of the epitaxial growth process. Sample numerical results have been presented for several transmission-line configurations and, when possible, compared with available published data, obtained by specialized techniques not easily extendable to conductors of arbitrary cross section.

VI. Appendix
Transmission Line Green's Functions

Consider a transmission-line network analogue of the layered medium of Fig. 1, formed by a tandem connection of transmission line sections, each corresponding to a dielectric layer (cf. Fig. 2). Let the network be excited by a 1 A current source located at z' in the nth line section. Then, the voltage and current at z within any line section, say the mth, satisfy the transmission-line equations [32]

$$\begin{cases} \dfrac{dV^p_{i,mn}}{dz} = -jk^p_{zm}Z^p_m I^p_{i,mn} \\ \dfrac{dI^p_{i,mn}}{dz} = -jk^p_{zm}Y^p_m V^p_{i,mn} + \delta(z-z') \end{cases} \tag{32}$$

where the propagation constant k^p_{zm} and characteristic impedance Z^p_m (and admittance Y^p_m) have been defined in (14) and (15), respectively. The superscript p, which stands for e or h, as explained in Section II, will henceforth be left out for brevity.

When $m = n$, i.e., the source and observation points are within the same nth line section, the voltage $V_{i,nm}$ is readily

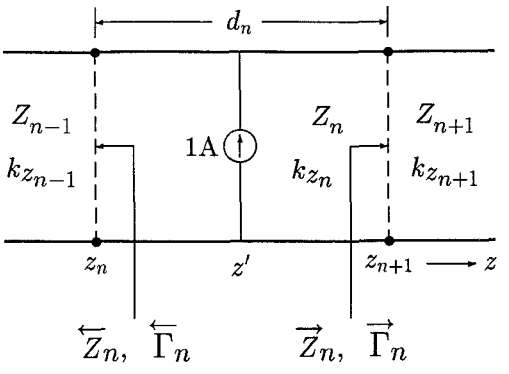

Fig. 11. Transmission line section containing a current source.

found from (32) as (cf. [32, p. 213], [26])

$$V_{i,nn}(z|z') = Z_n \frac{e^{-jk_{zn}|z-z'|}}{2W_n}[1 + \overleftarrow{\Gamma}_n e^{-j2k_{zn}(z_<-z_n)}] \cdot [1 + \overrightarrow{\Gamma}_n e^{-2k_{zn}(z_{n+1}-z_>)}] \tag{33}$$

where

$$W_n = 1 - \overleftarrow{\Gamma}_n \overrightarrow{\Gamma}_n e^{-j2k_{zn}d_n} \tag{34}$$

and $z_< \equiv \min(z, z'), z_> \equiv \max(z, z')$. In the above, $\overleftarrow{\Gamma}_n$ and $\overrightarrow{\Gamma}_n$ are the voltage reflection coefficients "looking to the left" and "looking to the right," respectively, at the two interior ends of this line section, as illustrated in Fig. 11. These reflection coefficients can be found as

$$\overleftarrow{\Gamma}_n = \frac{\overrightarrow{\overleftarrow{Z}}_n - Z_n}{\overrightarrow{\overleftarrow{Z}}_n + Z_n} \tag{35}$$

with the terminal impedances given by the recursive relations

$$\overrightarrow{\overleftarrow{Z}}_n = Z_{n\pm1} \frac{\overrightarrow{\overleftarrow{Z}}_{n\pm1} + jZ_{n\pm1}\tan(k_{z,n\pm1}d_{n\pm1})}{Z_{n\pm1} + j\overrightarrow{\overleftarrow{Z}}_{n\pm1}\tan(k_{z,n\pm1}d_{n\pm1})} \tag{36}$$

where the upper and lower signs correspond to the right and left arrows, respectively.

For $m \neq n$, $V_{i,mn}(z|z')$ is readily found from (32) and (33), by enforcing the continuity of the voltage and current at the interfaces. As a result, we obtain [26]

$$V_{i,mn}(z|z') = \begin{cases} V_{i,nn}(z_{n+1}|z')\overrightarrow{T}_{v,mn}(z), & n+1 \le m \le N \\ V_{i,nn}(z_n|z')\overleftarrow{T}_{v,mn}(z), & 1 \le m \le n-1 \end{cases} \tag{37}$$

where

$$\overrightarrow{T}_{v,mn}(z) = \frac{e^{-jk_{zm}(z-z_m)}}{1 + \overrightarrow{\Gamma}_m e^{-j2k_{zm}d_m}} \cdot [1 + \overrightarrow{\Gamma}_m e^{-j2k_{zm}(z_{m+1}-z)}] \cdot \prod_{i=n+1}^{m-1} \frac{(1+\overrightarrow{\Gamma}_i)e^{-jk_{zi}d_i}}{1 + \overrightarrow{\Gamma}_i e^{-j2k_{zi}d_i}} \tag{38}$$

$$\overleftarrow{T}_{v,mn}(z) = \frac{e^{-jk_{zm}(z_{m+1}-z)}}{1+\overleftarrow{\Gamma}_m e^{-j2k_{zm}d_m}} \cdot [1+\overleftarrow{\Gamma}_m e^{-j2k_{zm}(z-z_m)}] \cdot \prod_{i=m+1}^{n-1} \frac{(1+\overleftarrow{\Gamma}_i)e^{-jk_{zi}d_i}}{1+\overleftarrow{\Gamma}_i e^{-j2k_{zi}d_i}}. \quad (39)$$

It is understood in the above that the product terms are equal to one if the lower limits exceed the upper limits.

The transmission-line Green's functions can be efficiently implemented into a computer program, as explained below. First, we recognized that (33) may be written as

$$V_{i,nn}(z|z') = Z_n f_1(n; z; z'; \overleftarrow{\Gamma}_n; \overrightarrow{\Gamma}_n) \quad (40)$$

which serves to define the function f_1. The corresponding current can then easily be found from the first of (32) as

$$I_{i,nn}(z|z') = \pm f_2(n; z; z'; \pm\overleftarrow{\Gamma}_n; \pm\overrightarrow{\Gamma}_n), z \gtrless z' \quad (41)$$

which defines the function f_2. In a like manner, we may write (37) as

$$V_{i,mn}(z|z') = Z_n \begin{cases} f_1(n; z_{n+1}; z'; \overleftarrow{\Gamma}_n; \overrightarrow{\Gamma}_n) \cdot f_3[m; n; z; \overrightarrow{\Gamma}_j|_{(n<j\le m)}], & m > n \\ f_1(n; z_n; z'; \overleftarrow{\Gamma}_n; \overrightarrow{\Gamma}_n) \cdot f_4[m; n; z; \overleftarrow{\Gamma}_j|_{(m\le j<n)}], & m < n \end{cases} \quad (42)$$

which defines the functions f_3 and f_4. The corresponding current can again be found from the first of (32) as

$$I_{i,mn}(z|z') = \begin{cases} f_2(n; z_{n+1}; z'; \overleftarrow{\Gamma}_n; \overrightarrow{\Gamma}_n) \cdot f_3[m; n; z; -\overrightarrow{\Gamma}_j|_{(n<j\le m)}], & m > n \\ -f_2(n; z_n; z'; -\overleftarrow{\Gamma}_n; -\overrightarrow{\Gamma}_n) \cdot f_4[m; n; z; -\overleftarrow{\Gamma}_j|_{(m\le j<n)}], & m < n. \end{cases} \quad (43)$$

The current $I_{v,mn}$ and voltage $V_{v,mn}$, due to a unit-strength voltage source in the nth line section, satisfy a set of equations dual to (32). Hence, we may obtain these voltage and current transmission-line Green's functions from (40)–(43) by making the substitutions $V \to I, I \to V$, and $Z \to Y$. Note that the last substitution causes all reflection coefficients to change signs. We observe that only four subroutines, corresponding to the functions f_1 through f_4, are required to implement all the transmission-line Green's functions in the computer code.

REFERENCES

[1] F. E. Gardiol, "Design and layout of microstrip structures," *Proc. Inst. Elec. Eng.*, vol. 135, pt. H, pp. 145–157, June 1988.

[2] W. Schroeder and I. Wolff, "A new hybrid mode boundary integral method for analysis of MMIC waveguides with complicated cross-section," in *1989 IEEE MTT-S Int. Microwave Symp. Dig.*, Long Beach, CA, pp. 711–714.

[3] N. Alexópoulos, "Integrated-circuit structures on anisotropic substrates," *IEEE Trans. Microwave Theory Tech.*, vol. MTT-33, pp. 847–881, Oct. 1985.

[4] E. J. Denlinger, "A frequency dependent solution for microstrip transmission lines," *IEEE Trans. Microwave Theory Tech.*, vol. MTT-19,pp. 30–39, Jan. 1971.

[5] T. Itoh and R. Mittra, "Spectral-domain approach for calculating the dispersion characteristics of microstrip lines," *IEEE Trans. Microwave Theory Tech.*, vol. MTT-21, pp. 496–499, June 1973.

[6] G. Kowalski and R. Pregla, "Dispersion characteristics of single and coupled microstrips," *Arch. Elek. Übertragung.*, vol. 26, no. 6, pp. 276–280, 1972.

[7] {—}{—}, "Dispersion characteristics of single and coupled microstrips with double-layer substrates," *Arch. Elek. Übertragung.*, vo. 27, no. 3, pp. 125–130, 1973.

[8] Y. Hayashi and T. Kitazawa, "Analysis of microstrip transmission line on a sapphire substrate," *J. Inst. Electron. Commun. Eng. Jap.*, vol. 62-B, no. 6, pp. 64–71, 1979.

[9] A. M. A. El-Sherbiny, "Hybrid mode analysis of microstrip lines on anisotropic substrates," *IEEE Trans. Microwave Theory Tech.*, vol. MTT-29, pp. 1261–1266, Dec. 1981.

[10] T. Kitazawa and Y. Hayashi, "Propagation characteristics of striplines with multilayered anisotropic media," *IEEE Trans. Microwave Theory Tech.*, vol. MTT-31, pp. 429–433, June 1983.

[11] F. Medina and M. Horno, "Determination of Green's function matrix for multiconductor and anisotropic multidielectric planar transmission lines: A variational approach," *IEEE Trans. Microwave Theory Tech.*, vol. MTT-33, pp. 933–940, Oct. 1985.

[12] B. E. Kretch and R. E. Collin, "Microstrip dispersion including anisotropic substrates," *IEEE Trans. Microwave Theory Tech.*, vol. MTT-35, pp. 710–718, Aug. 1987.

[13] N. Faché and D. De Zutter, "Rigorous full-wave space-domain solution for dispersive microstrip lines," *IEEE Trans. Microwave Theory Tech.*, vol. 36, pp. 731–737, Apr. 1988.

[14] N. Faché, J. Van Hese, and D. De Zutter, "Generalized space domain Green's dyadic for multilayered media with special application to microwave interconnections," *J. Electromagn. Waves Appl.*, vol. 3, pp. 651–669, July 1989.

[15] T. Kitazawa, "Variational method for multiconductor coupled striplines with stratified anisotropic media," *IEEE Trans. Microwave Theory Tech.*, vol. 37, pp. 484–491, Mar. 1989.

[16] Y. Yuan and D. P. Nyquist, "Full-wave perturbation theory based upon electric field integral equations for coupled microstrip transmission lines," *IEEE Trans. Microwave Theory Tech.*, vol. 38, pp. 1576–1584, Nov. 1990.

[17] K. A. Michalski and D. Zheng, "A spectral-domain method for the analysis of the fundamental-mode leakage effect in microstrip lines on uniaxial substrate," *Microwave and Opt. Technol. Lett.*, vol. 4, no. 4, pp. 158–161, 1991.

[18] J F. Kiang, "Integral equation solution to the skin effect problem in conductor strips of finite thickness," *IEEE Trans. Microwave Theory Tech.*, vol. 39, pp. 452–460, Mar. 1991.

[19] K. A. Michalski and D. Zheng, "Rigorous analysis of open microstrip lines of arbitrary cross section in bound and leaky regimes," *IEEE Trans. Microwave Theory Tech.*, vol. 37, pp. 2005–2010, Dec. 1989.

[20] C. F. Railton and J. P. McGeehan, "An analysis of microstrip with rectangular and trapezoidal conductor cross sections," *IEEE Trans Microwave Theory Tech.*, vol. 38, pp. 1017–1022, Aug. 1990.

[21] N. Faché and D. De Zutter, "Full-wave analysis of a perfectly conducting wire transmission line in a double-layered conductor-backed medium," *IEEE Trans. Microwave Theory Tech.*, vol. 37, pp. 512–518, Mar. 1989.

[22] N. Faché, F. Olyslager, and D. De Zutter, "Full-wave analysis of coupled perfectly conducting wires in a multilayered medium," *IEEE Trans. Microwave Theory Tech.*, vol. 39, pp. 673–680, Apr. 1991.

[23] M. Chryssomallis and J. N. Sahalos, "An analytic method to study open thick microstrips," *Arch. Elektrotech.*, vol. 72, no. 4, pp. 283–291, 1989.

[24] K. C. Gupta, R. Garg, and I. J. Bahl, *Microstrip Lines and Slotlines*. Dedham, MA: Artech House, 1979.

[25] J. R. Mosig and F. E. Gardiol, "A dynamical radiation model for microstrip structures," in *Adv. Electron. Electron Phys.*, P. W. Hawkes, Ed., vol. 59, pp. 139–237, New York: Academic Press, 1982.

[26] K. A. Michalski and D. Zheng, "Electromagnetic scattering and radiation by surfaces of arbitrary shape in layered media. Part I: Theory," *IEEE Trans. Antennas Propagat.*, vol. 38, pp. 335–344, Mar. 1990.

[27] K. A. Michalski and C.-I. G. Hsu, "Formulation of mixed-potential integral equations for arbitrarily shaped microstrip structures," *J. Electromagn. Waves Appl.*, accepted for publication.

[28] R. F. Harrington, *Field Computation by Moment Methods*. New York: Macmillan, 1968; reprinted by Krieger Publishing Co., Melbourne, FL, 1982.

[29] A. W. Glisson and D. R. Wilton, "Simple and efficient numerical

methods for problems of electromagnetic radiation and scattering from surfaces," *IEEE Trans. Antennas Propagat.*, vol. AP-28, pp. 593–603, Sept. 1980.
[30] K. A. Michalski, "On the scalar potential of a point charge associated with a time-harmonic dipole in a layered medium," *IEEE Trans. Antennas Propagat.*, vol. AP-35, pp. 1299–1301, Nov. 1987.
[31] K. A. Michalski, "The mixed-potential electric field integral equation for objects in layered media," *Arch. Elek. Übertragung.*, vol. 39, pp. 317–322, Sept.–Oct. 1985.
[32] L. B. Felsen and N. Marcuvitz, *Radiation and Scattering of Waves.* Englewood Cliffs, NJ: Prentice-Hall, 1973.
[33] N. K. Das and D. M. Pozar, "A generalized spectral-domain Green's function for multilayer dielectric substrates with application to multilayer transmission lines," *IEEE Trans. Microwave Theory Tech.*, vol. MTT-35, pp. 326–335, Mar. 1987.
[34] J. R. Mosig and F. E. Gardiol, "Analytic and numerical techniques in the Green's function treatment of microstrip antennas and scatterers," *Proc. Inst. Elec. Eng.*, vol. 130, Pt. H, pp. 175–182, Mar. 1983.
[35] S. D. Conte and C. de Boor, *Elementary Numerical Analysis: An Algorithmic Approach.* New York: McGraw-Hill, 1980.
[36] H. Shigesawa, M. Tsuji, and A. A. Oliner, "Dominant mode power leakage from printed-circuit waveguides," *Radio Sci.*, vol. 26, no. 2, pp. 559–564, 1991.
[37] G. Goubau, "Single-conductor surface-wave transmission lines," *Proc. IRE*, vol. 39, pp. 619–624, June 1951.

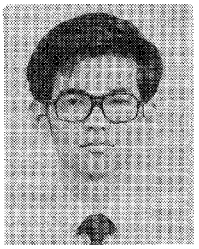

Chung-I G. Hsu (S'87–M'92) graduated from National Taipei Institute of Technology, Taiwan, in 1980. He received the M.Sc. degree from The University of Mississippi in 1986, and the Ph.D. degree from Syracuse University in 1991. He spent the Spring 1992 semester at the Microwave and Electromagnetics Laboratory, Texas A&M University, doing research on the modeling of microstrip antennas.

Roger F. Harrington (S'48–A'53–M'57–SM'62–F'68–LF'91) was born in Buffalo, NY on December 24, 1925. He received the B.E.E. and M.E.E. degrees from Syracuse University, Syracuse, NY, in 1948 and 1950, respectively, and the Ph.D. degree from Ohio State University, Columbus, in 1952.

From 1945 to 1946 he served as an Instructor at the U.S. Naval Radio Materiel School, Dearborn, MI, and from 1948 to 1950 he was employed as an Instructor and Research Assistant at Syracuse University. While studying at Ohio State University, he served as a Research Fellow in the Antenna Laboratory. Since 1952, he has been on the faculty of Syracuse University, where he is presently Professor of Electrical Engineering. During the years 1959–1960 he was Visiting Associate Professor at the University of Illinois, Urbana; in 1964 he was Visiting Professor at the University of California, Berkeley; and in 1969 he was Guest Professor at the Technical University of Denmark, Lyngby.

Dr. Harrington is a member of Tau Beta Pi, Sigma Xi, and the American Association of University Professors.

Krzysztof A. Michalski (S'78–M'81–SM'88) received the M.Sc. degree from the Technical University of Wrocław, Poland, in 1974, and the Ph.D. degree from the University of Kentucky in 1981. From 1982 to 1986, he was Assistant Professor at The University of Mississippi. Since 1987, he has been Associate Professor of Electrical Engineering at Texas A&M University.

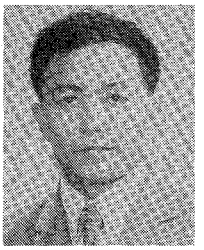

Dalian Zheng (S'85–M'89) received the B.Sc. degree from the Beijing Institute of Aeronautics and Astronautics, China, in 1982, the M.Sc. degree from The Ohio State University in 1985, and the Ph.D. degree from The University of Mississippi in 1988. From 1989 to 1991, he was Research Associate at the Microwave and Electromagnetics Laboratory, Texas A&M University. He is currently with Integrated Engineering Software, Inc., Winnipeg, Manitoba.